PCCP

Cite this: *Phys. Chem. Chem. Phys.*, 2011, **13**, 15546–15553

www.rsc.org/pccp

PAPER

Electronic and magnetic properties of perfect, vacancy-doped, and nonmetal adsorbed $MoSe_2$, $MoTe_2$ and WS_2 monolayers

Yandong Ma, Ying Dai,* Meng Guo, Chengwang Niu, Jibao Lu and Baibiao Huang

Received 13th April 2011, Accepted 28th May 2011
DOI: 10.1039/c1cp21159e

Very recently, two-dimensional nanosheets of $MoSe_2$, $MoTe_2$ and WS_2 were successfully synthesized experimentally [*Science*, 2011, **331**, 568]. In the present work, the electronic and magnetic properties of perfect, vacancy-doped, and nonmetal element (H, B, C, N, O, and F) adsorbed $MoSe_2$, $MoTe_2$ and WS_2 monolayers are systematically investigated by means of first-principles calculations to give a detailed understanding of these materials. It is found that: (1) $MoSe_2$, $MoTe_2$ and WS_2 exhibit surprising confinement-induced indirect-direct-gap crossover; (2) among all the neutral native vacancies of $MoSe_2$, $MoTe_2$ and WS_2 monolayers, only the Mo vacancy in $MoSe_2$ can induce spin-polarization and long-range antiferromagnetic coupling; (3) adsorption of nonmetal elements on the surface of $MoSe_2$, $MoTe_2$ and WS_2 nanosheets can induce a local magnetic moment; H-absorbed WS_2, $MoSe_2$, and $MoTe_2$ monolayers and F-adsorbed WS_2 and $MoSe_2$ monolayers show long-range antiferromagnetic coupling between local moments even when their distance is as long as $\sim$12 Å. These findings are a useful addition to the experimental studies of these new synthesized two-dimensional nanosheets, and suggest a new route to facilitate the design of spintronic devices for complementing graphene. Further experimental studies are expected to confirm the attractive predictions.

I. Introduction

Two-dimensional (2D) materials are attractive for use in next-generation nanoelectronic devices because, compared to one-dimensional materials, it is easy to fabricate complex structures from them, such as quantum wells, multilayers, superlattices, and heterostructures. One kind of important two-dimensional materials, 2D transition metal dichalcogenides (TMDs) with thickness down to two or three atomic layers, is of particular interest due to their distinctive electronic, optical, and catalytic properties, as well as their importance for complementing graphene in applications requiring thin transparent semiconductors.[1–4] In fact, the 2D TMDs monolayer has attracted broad interest both experimentally and theoretically during recent years.[1,5–15] Very recently, Jonathan *et al.*[5] firstly synthesized $MoSe_2$ and $MoTe_2$ single layers and indicated that layered compounds, such as $MoSe_2$, $MoTe_2$ and WS_2, can be efficiently dispersed in common solvents and deposited as individual flakes or formed into films, which suggests that these materials can be exfoliated into monolayers. Despite progress in the experimental fabrication of TMDs monolayer and theoretical investigation of the bulk materials, detailed theoretical understanding of the electronic structure and related properties of these new two-dimensional systems is absent. In addition, Mak *et al.*[7] demonstrated that the indirect band gap of bulk MoS_2 becomes direct in few-layer flakes, namely, quantum confinement effect occurs in layered d-electron materials like MoS_2, which may provide new opportunities for engineering the electronic structure of matter at the nanoscale. Therefore, it is interesting to investigate the related quantum confinement effect of other single-layer TMDs, such as $MoSe_2$, $MoTe_2$ and WS_2. Furthermore, it is well-known that the native defects typically depend on the growth conditions, as well as on the presence of chemical impurities and could influence the electronic properties significantly. It is therefore desirable to study the properties of native defects in 2D TMDs, whereas, up to now no theoretical calculations have been performed to study the effects of native defects on the properties of TMDs single-layers. Moreover, it seems that magnetism can not be induced by native defects in MoS_2 monolayer, therefore it becomes intriguing if the native defects in other potential 2D TMDs could induce spin-polarization.

The advance in experimental synthesis such 2D structures[5] encourages us to explore their properties by decorating their surface. And previous studies have found that the adsorption

School of Physics, State Key Laboratory of Crystal Materials, Shandong University, Jinan 250100, People's Republic of China. E-mail: daiy60@sina.com

of nonmetal element on the surface of low-dimensional systems can induce a local magnetic moment.[6,16–19] Compared with the magnetic moment from d- or f-electrons of transition metal atoms, the magnetism based on sp states of a nonmetal element are of some obvious advantage, such as stronger long-range exchange coupling interactions and no clustering of magnetic ions.[20,21] Compared with the wide research on functionalized graphene, less attention has hitherto been paid to the electronic structures and magnetic properties of single atom adsorbed TMDs monolayers such as $MoSe_2$, $MoTe_2$ and WS_2 nanosheets.

Motivated by the questions above, in the present work we systematically study the geometric structure, electronic structure, and magnetic behavior of $MoSe_2$, $MoTe_2$ and WS_2 monolayers without and with native defects including cation vacancy and anion vacancy, as well as the related properties of H-, B-, C-, N-, O-, and F-adsorbed $MoSe_2$, $MoTe_2$ and WS_2 monolayers, by means of density functional theory calculations. It is shown that $MoSe_2$, $MoTe_2$ and WS_2 crystals exhibit a crossover from an indirect- to direct-gap semiconductor in the monolayer limit; only the cation vacancy can induce spin-polarization in $MoSe_2$ monolayer whereas not in $MoTe_2$ and WS_2 monolayers; H-absorbed WS_2, $MoSe_2$, and $MoTe_2$ and F-adsorbed WS_2 and $MoSe_2$ monolayer sheets show long-range antiferromagnetic ordering. We hope the interesting properties predicted by this study will promote efforts towards the understanding of these new materials.

II. Computational methods

Spin-polarized density functional theory (DFT) calculations were performed using the projector-augment wave[22] method with a plane-wave basis set as implemented in the Vienna *ab initio* simulation package (VASP) code.[23–25] The plane-wave cutoff energy was 400 eV and the exchange–correlation functional was treated by Perdew–Burke–Ernzerhof from generalized gradient approximation (GGA).[26] The $MoSe_2$, $MoTe_2$ and WS_2 monolayers were modeled by 4×4 and 8×4 unit cells, which contain 48 and 96 atoms, respectively. The distance between two adjacent adatoms or vacancies is above 12.74 Å and hence the interaction between them can be ignored. The distance between two adjacent monolayers is larger than 15 Å to avoid the layer–layer interaction. For the Brillouin-zone sampling, 5×5×1 Monkhorst–Pack[27] k mesh was used for the 4×4 unit cells while 3×4×1 k mesh was used for the 8×4 unit cells. The structure relaxations were carried out until all the atomic forces on each ion were less than 0.02 eV $Å^{-1}$. Because Mo and W are not strongly correlated systems, a relative small value of the on-site Coulomb interaction is sufficient for them, therefore recent theoretical studies on 2D Mo systems[6,9,15] usually neglected the GGA + U method. And some of our results are also tested in the GGA + U method with U = 1.0 eV, which do not affect the main conclusions based on GGA method. Thus, in order to compare with the previous work,[6,9,15] we employ the GGA method in the present work.

The formation energy of the native vacancy in $MoSe_2$, $MoTe_2$ and WS_2 monolayers is calculated as $E_f = E_{total} - E_{monolayer} + E_i$, where E_{total} and $E_{monolayer}$ are the total energies of the monolayer with and without vacancies. E_i is the chemical potential for host atoms, which depends on the material growth conditions and satisfies the boundary conditions. While the adsorption energy (E_{ads}) of the adatom on the surface of $MoSe_2$, $MoTe_2$ and WS_2 monolayers is defined as $E_{ads} = E_{total} - E_{monolayer} - E_{atom}$ in terms of the total energy of the whole adsorbed system (E_{total}), the pristine monolayer ($E_{monolayer}$), and the free atom (E_{atom}). We employ the same method as ref. 28 and 29 to calculate the chemical potentials for host atoms and adatoms (*i.e.* the energies of isolated H, B, C, N, O, F, S, Se, Te, Mo, and W atoms, respectively).

III. Results and discussions

3.1 Geometric structure and band structure of perfect MX_2

For the convenience of our discussion, we denote the $MoSe_2$, $MoTe_2$ and WS_2 monolayers as MX_2 (MX_2 = $MoSe_2$, $MoTe_2$, WS_2). The crystalline structure of perfect MX_2 4×4 supercell is plotted in Fig. 1 and the corresponding calculated geometric parameters are listed in Table 1. As shown in Table 1, the crystal structure of MX_2 monolayer is similar to the single layer of bulk MX_2,[30–32] except that the internal parameters differ slightly. Generally, M is in a 4+ state due to the donation of its four valence electrons to the neighboring X atoms with 2− state.

The band structure, total density of states (TDOS) and partial density of states (PDOS) of perfect MX_2 monolayer are calculated and shown in Fig. 2 to explore its electronic properties. Similar to three-dimensional MX_2,[30–32] the MX_2 monolayer is of semiconductor character, the band edges are derived mainly from the M-d states and the bands show strong hybridization of M-d and X-p orbitals, which can be ascribed

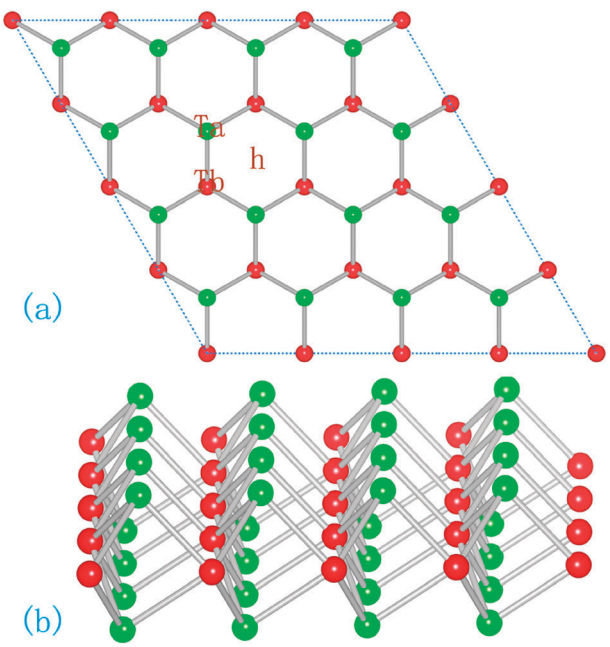

Fig. 1 Top (a) and side (b) views of atomic structures of TMD monolayer. The red and green balls represent M (M = W, Mo) and X (X = S, Se, Te) atoms, respectively. There are three different absorption sites: *Ta*, *Tb*, and *h*, which stand for the positions above the X atom, M atom, and the center of the hexagonal ring of MX_2 monolayer, respectively.

Table 1 Calculated lattice constant (a), buckled height between two X atom planes (Δ), M–X bond length (d_{M-X}), X–M–X bond angle (θ), and band gap (E_g) values for optimized MX_2 monolayer

	a/Å	Δ (Å)	d_{M-X} (Å)	θ (X–M–X)	E_g (eV)
$MoSe_2$	3.319	3.34	2.54	81.56°	1.44
$MoTe_2$	3.552	3.61	2.73	81.06°	1.07
WS_2	3.184	3.14	2.42	82.39°	1.80

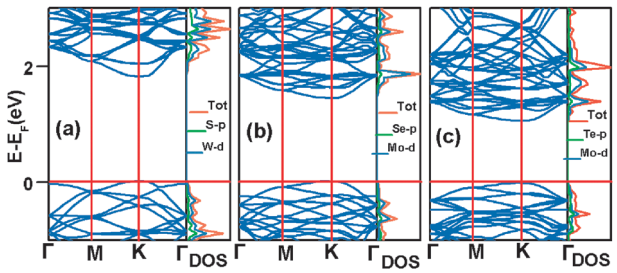

Fig. 2 Band structure and TDOS of monolayer WS_2 (a), $MoSe_2$ (b), and $MoTe_2$ (c). PDOS on inequivalent atoms are also presented with different colors.

to the absence of significant structure variation from three-dimensional to two-dimensional, and hence the electronic structure of the monolayer is affected slightly. Furthermore, since the reduced dimensionality can sometimes result in magnetic behavior in systems which are not magnetic in bulk, we check the possibility a spin-polarized ground state. The calculated DOS displays spin unpolarized with symmetric characteristic for the majority and minority projections of the spin (not shown in this paper). The total magnetic moments of these systems are zero, indicating the local magnetic moment cannot form in a perfect MX_2 monolayer. Therefore, at this point, the perfect MX_2 is nonmagnetic.

As suggested by previous calculations,[7,9,33,34] the MoS_2 crystal exhibits a crossover from an indirect- to direct-gap semiconductor in the monolayer limit. As an evidence of this effect, unlike the bulk material, the MoS_2 monolayer emits light strongly, and the freestanding monolayer exhibits an increase in luminescence quantum efficiency by more than a factor of 10^4 compared with the bulk material. Since the indirect-direct-gap crossover can be induced by the effect of quantum confinement for MoS_2, it is appropriate to investigate the relevant electronic properties of $MoSe_2$, $MoTe_2$ and WS_2 monolayers. Surprisingly, the band structures of MX_2 monolayers shown in Fig. 2 indicate that, the same as MoS_2, all three materials display indirect-direct-gap crossover character. It is evident that the monolayer sheets are semiconductors with direct band gaps of 1.80, 1.44, and 1.07 eV for WS_2, $MoSe_2$, and $MoTe_2$ monolayers, respectively, whereas for the three-dimensional MX_2 the bands are indirect,[30–32] which indicates the quantum confinement-induced indirect-direct-gap crossover character also appears in WS_2, $MoSe_2$, and $MoTe_2$. For these three monolayers, the band edges all locate at the high symmetry point K. It is thus concluded that WS_2, $MoSe_2$, and $MoTe_2$ monolayers may exhibit an increase in luminescence quantum efficiency, which suggests their potential use for photostable markers and sensors in probing nanoscale dimensions. By the way, the controllability of the band gap may also be used to optimize the material's applications as a photocatalytic agent and for photovoltaic devices.[2] Our results imply that the distinctive electronic properties of atomically thin layered materials are not restricted to graphene but extend to a broader group of van der Waals bonded solids. It is important that this interesting confinement-induced shift is not limited to WS_2, MoS_2, $MoSe_2$, and $MoTe_2$, which is also expected to be applicable to other classes of TMDs, thus highlighting a new direction for further studies.

3.2 Effect of the vacancy on the electronic and magnetic properties of MX_2

Next, the magnetic properties of the undoped MX_2 monolayer are studied. Generally, there are two kinds of possible native

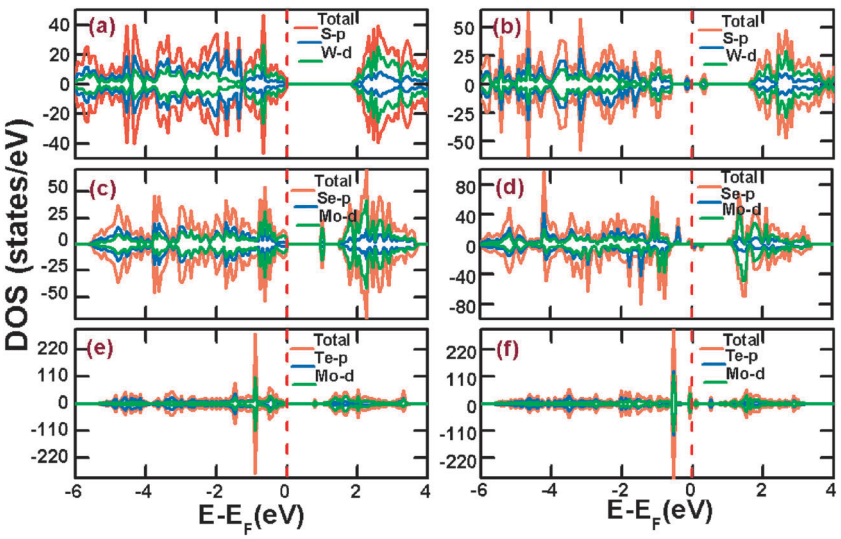

Fig. 3 The total DOS and the corresponding PDOS of (a) WS_2 monolayer with one S vacancy; (b) WS_2 monolayer with one W vacancy; (c) $MoSe_2$ monolayer with one Se vacancy; (d) $MoSe_2$ monolayer with one Mo vacancy; (e) $MoTe_2$ monolayer with one Te vacancy; (f) $MoTe_2$ monolayer with one Mo vacancy. The vertical dashed line represents the Fermi level.

point vacancies in the MX_2 monolayer, which are M vacancy (V_M) and X vacancy (V_X). Though the charge states of the native vacancies in the MX_2 monolayer can be 0, −2, +4, only the neutral native vacancies are considered in this paper. First, the effect of X vacancies on the magnetic properties of MX_2 monolayer is studied by generating one X vacancy (V_X) in the 4×4 supercell, which leads to X-vacancy concentration of 3.125%. After full relaxation, the three nearest M atoms move inwards slightly by only 0.03, 0.02, and 0.06 Å with respect to the vacancy site for $MoSe_2$, $MoTe_2$, and WS_2 monolayers, respectively. The total DOS and the corresponding PDOS of the MX_2 monolayer with one X vacancy are shown in Fig. 3(a), (c) and (e). In the presence of anion vacancy, the DOS remains spin unpolarized and the total magnetic moment of the system is zero. Generally, one X vacancy as a donor can introduce two electrons to the system. For $MoSe_2$ and $MoTe_2$ monolayer sheets, an unoccupied impurity state of X vacancy appears in the band gap, which does not destroy the semiconducting behavior but decreases the band gap. The formation energies of $MoSe_2$, $MoTe_2$, and WS_2 monolayers with the X vacancy are calculated to be 6.08, 5.37, and 4.94 eV, respectively. To further investigate the effect of X vacancies concentration, one X atom is also removed in the 2×4 supercell, corresponding to the X-vacancy concentration of 6.25%. This system does not exhibit a local magnetic moment, which suggests that neutral X vacancies do not induce magnetism in MX_2 monolayer independent of concentration.

For the undoped MX_2 with one M vacancy (V_M), which is obtained by removing one M atom from 4×4 supercell corresponding to a concentration of 6.25%, the calculated DOS are shown in Fig. 3(b), (d) and (f). For $MoTe_2$ and WS_2 monolayers, the M vacancy induces spin unpolarization. It seems that the native vacancy in the undoped MX_2 monolayer could not induce a magnetic moment irrespective of the kinds of the possible native point vacancies. Yet, differently, it is exciting that Mo vacancies will introduce strong spin polarization and lead to the formation of local moments in the $MoSe_2$ monolayer [see Fig. 3(d)]. In principle, one Mo vacancy as an acceptor can leave four holes in the system and the total magnetic moments should be 4 μ_B, however, the calculated total magnetic moment are 3.27 μ_B. The decrease in magnetic moment is due to the large relaxation of the next-neighbor Se atoms. The main contribution to the total magnetic moment arises from the p orbital of the six nearest Se atoms (0.30 μ_B) and the d orbital of six next-neighboring Mo atoms (0.19 μ_B). The other atoms in the supercell also have a little contribution to the moment (*i.e.* 0.012 μ_B, 0.004 μ_B). Compared to the perfect $MoSe_2$ monolayer, some impurity states appear in the gap, resulting in an asymmetric spin-up and spin-down DOS near the Fermi energy. As shown in Fig. 3(d), the local moment is mainly contributed by the p orbital of the Se atoms and the d orbital of Mo atoms. The strong spin polarization can also be visualized by plotting the defect states spin density in the real spaces. Fig. 4 shows an isosurface plot of the spin density of $MoSe_2$ monolayer with one Mo vacancy. It is evident that the spin polarization is strongly localized on the nearest Se atoms and the next-neighboring Mo atoms. It is this localized spin polarization that leads to the formation of the magnetic moment in this system.

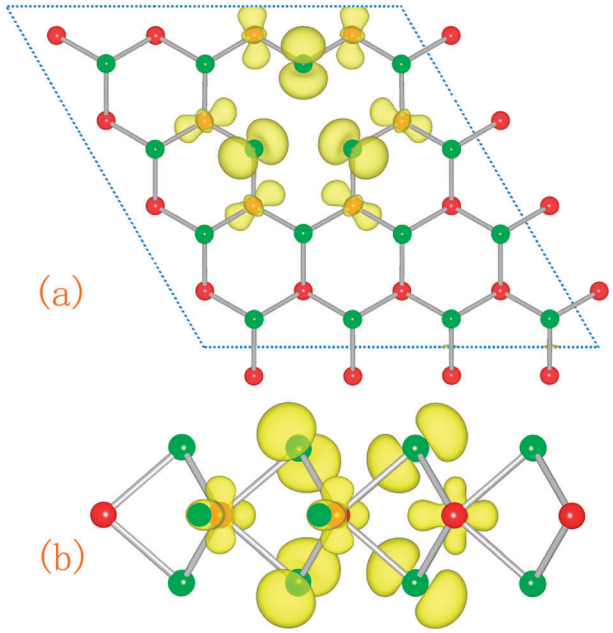

Fig. 4 Top (a) and side (b) views of the isosurface plot of the spin density of $MoSe_2$ monolayer with one Mo vacancy. The red and green balls represent Mo and Se atoms, respectively. The blue isosurface shows the spin density.

The existence of the magnetic moment does not certainly result in magnetic coupling. It is thus necessary to study the magnetic coupling between the vacancy-induced moments. We doubled the size of the previous supercell in *x* direction, and each supercell now contains two Mo vacancies, indicating that the distance between two adjacent vacancies is about 13 Å. Depending on the initial conditions of self-consistent calculations, two stable magnetic structures are obtained: one is ferromagnetic (FM) and the other antiferromagnetic (AFM).

Table 2 Distance (Å) between the adatom and the S atom (d_{S-Ad}) and W atom (d_{W-Ad}), absorbed energy (E_{ads}, in eV), and the magnetic moments (μ_B) of the whole system (μ_{total}) and the adatom (μ_{adatom}) for each most stable configuration of the nonmetal adsorbed WS_2 monolayer

Adatoms position	H *Ta*	B *Tb*	C *Tb*	N *Ta*	O *Ta*	F *Ta*
d_{S-Ad}	1.434	1.866	1.805	1.521	1.486	1.888
d_{W-Ad}	...	2.162	2.082	...	...	...
E_{ads}	−0.103	−2.257	−1.788	−1.241	−3.830	−1.829
μ_{total}	1	1	2	1	...	1
μ_{adatom}	0.05	0.03	0.04	0.49	...	0.295

Table 3 Distance (Å) between the adatom and the Se atom (d_{Se-Ad}) and Mo atom (d_{Mo-Ad}), absorbed energy (E_{ads}, in eV), and the magnetic moments (μ_B) of the whole system (μ_{total}) and the adatom (μ_{adatom}) for each most stable configuration of the nonmetal adsorbed $MoSe_2$ monolayer

Adatoms position	H *Ta*	B *Tb*	C *Tb*	N *Ta*	O *Ta*	F *Ta*
d_{Se-Ad}	1.569	1.997	1.953	1.670	1.671	2.004
d_{Mo-Ad}	...	2.147	2.087	...	...	...
E_{ads}	−0.021	−2.815	−2.599	−0.714	−3.160	−2.101
μ_{total}	1	1	2	1	...	1
μ_{adatom}	0.05	0.01	0.02	0.62	...	0.27

Table 4 Distance (Å) between the adatom and the Te atom ($d_{Te–Ad}$) and Mo atom ($d_{Mo–Ad}$), absorbed energy (E_{ads}, in eV), and the magnetic moments (μ_B) of the whole system (μ_{total}) and the adatom (μ_{adatom}) for each most stable configuration of the nonmetal adsorbed $MoTe_2$ monolayer

Adatoms position	H *h*	B *Tb*	C *Tb*	N *Tb*	O *Ta*	F *h*
$d_{Te–Ad}$	2.230	2.190	2.149	2.206	1.849	2.581
$d_{Mo–Ad}$	...	2.133	2.093	2.199	...	...
E_{ads}	−0.536	−2.997	−3.227	−1.067	−3.411	−2.652
μ_{total}	1	1	2	1	...	...
μ_{adatom}	0.09	0.01	0.06	0.14	...	...

It is found that the magnetic coupling between the two vacancies can still be observed even at such a long distance, resulting from the large spatial extensions of spin density just discussed above. Total energy calculations show that the energy difference, ΔE, between the FM and AFM phases is $E_{FM} - E_{AFM} = 1.5$ meV. To drive the strength of the exchange coupling, the Heisenberg model, $H = -J\sum_i \sigma_i\sigma_{i+1}$, is employed, where J is the exchange coupling parameter, and σ_i is the net spin induced by the ith vacancy. Comparing this result with ΔE from *ab initio* calculations, a positive exchange coupling $J = -3.0$ meV is yielded in this system, indicating a weak antiferromagnetic coupling. We can assign this small value of J as the long spatial distance of 13.276 Å between the two vacancies. Although the Curie temperature is not too high at such a long coupling distance, the results provide an interesting potential way to obtain long-range magnetic coupling. Of course, the Curie temperature can be significantly increased to room temperature by reducing the distance between the local magnetic moments.

At last, the charge injection effect should be clarified to discuss the magnetic properties in the vacancy-doped MX_2 nanosheet. It is known that the charge injection into the vacancy-doped MX_2 nanosheet should drastically affect its magnetism.[35–38] When two holes are doped in the V_X-doped MX_2 nanosheet (corresponding to V_X^{2-}-doped MX_2), the spin is induced. The calculated magnetic moments are about 1.02,

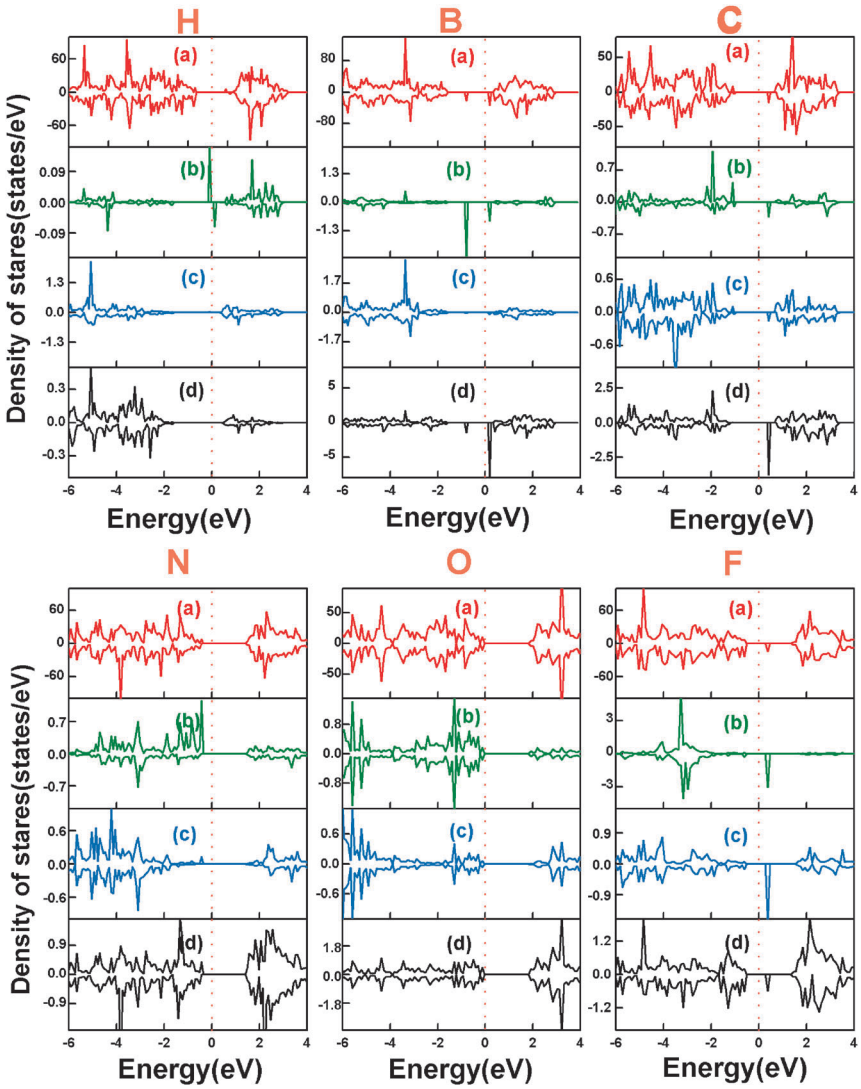

Fig. 5 The total DOS and the corresponding PDOS of H-, B-, C-, N-, O-, and F-adsorbed WS_2 monolayers. The upper most plane is the total DOS (a). The planes of (b), (c), and (d) are the p states of adatom (s states for H), p states of the nearest S atom, and d states of the nearest W atom, respectively. The vertical dashed line represents the Fermi level.

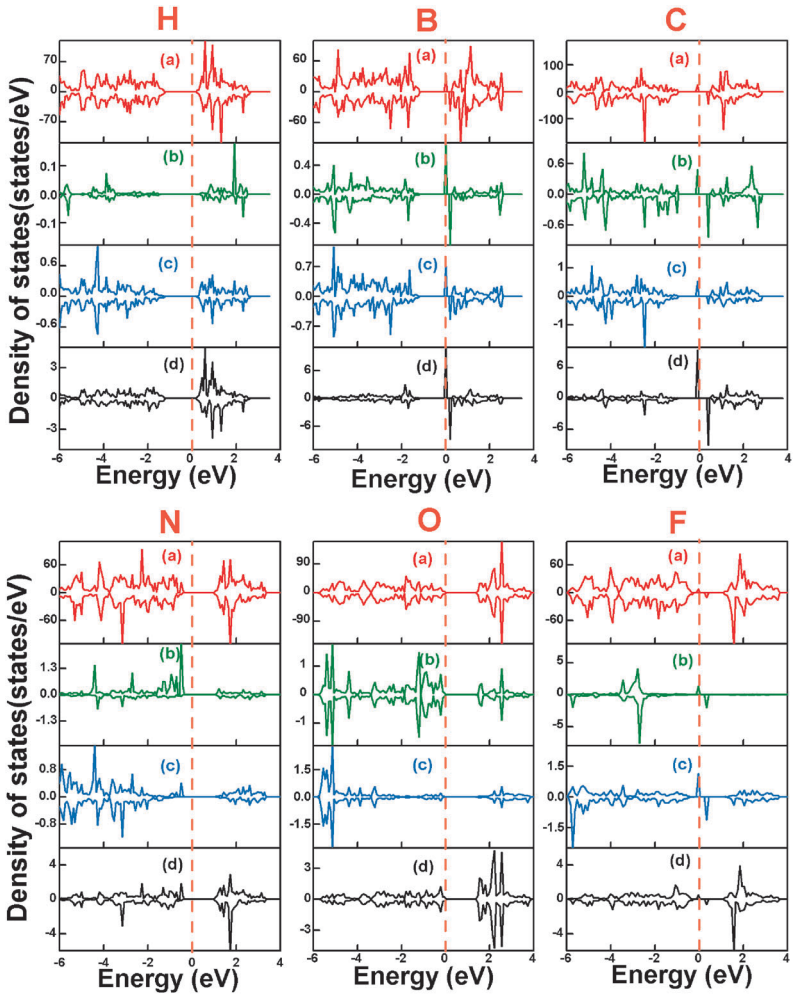

Fig. 6 The total DOS and the corresponding PDOS of H-, B-, C-, N-, O-, and F-adsorbed $MoSe_2$ monolayers. The upper most plane is the total DOS (a). The planes of (b), (c), and (d) are the p states of adatom (s states for H), p states of nearest Se atom, and d states of the nearest Mo atom, respectively. The vertical dashed line represents the Fermi level.

0.85, and 0.13μ_B for V_X^{2-}-doped $MoSe_2$, $MoTe_2$, and WS_2 monolayers, respectively. And when four electrons are doped in the V_M-doped $MoTe_2$ and WS_2 nanosheets (corresponding to V_M^{4+}-doped $MoTe_2$ and WS_2), resemble the V_X^{2-}-doped MX_2 cases, V_M^{4+} will introduce spin polarization, and the corresponding magnetic moments are 1.21 and 0.58 μ_B, while for the V_{Mo}^{4+}-doped $MoSe_2$ case, the magnetic moments are weakened to 2.14 μ_B, lower than the case without electron doping. These results suggest an experimentally viable way for tailoring magnetism in the vacancy-doped MX_2 nanosheet. Similar control of magnetism has been demonstrated in the wide-gap nitrides with cation-vacancy.[38]

3.3 Geometric and electronic structure and magnetism of nonmetal element adsorbed MX_2 monolayer

Surface decorating of these sheets may result in fantastic properties, to study the effect of nonmetal element (H, B, C, N, O, and F) adsorption on the electronic properties and magnetism of MX_2 monolayer, we consider only one atom adsorbed on the perfect MX_2 4×4 supercell. The distance between two adjacent adatoms is above 12.74 Å and hence the interaction between them can be ignored. To search the most stable configuration, as shown in Fig. 1(a), we considered three possible adsorbed structures *Ta*, *Tb*, and *h*, namely, the nonmetal atom occupies the ontop position of the X site of *Ta*, M site of *Tb*, and the hollow site of *h*. All the initial arrangements of the three structures were fully relaxed, and the formation energies are calculated using the optimized structures. For each adatom, the most energetically favorable adsorbed position is listed in Tables 2, 3, and 4, corresponding with its adsorption energy. For WS_2 and $MoSe_2$ monolayers, it is clear that the H, N, O, and F atoms favor the site of *Ta*, while the *Tb* is the most stable position to be adsorbed for B and C. All these adatoms do not favor *h* site due to the large size of the honeycomb formed by three X and three Mo atoms. Following this trend, the most stable sites for these atoms are *Ta* or *Tb*. However, for the $MoTe_2$ monolayer, the absorption energy is the lowest for H or F atom absorbed at *h* site. One possible explanation of the contradiction might be the slight electronegativity difference between Te (2.1) and Mo (2.16) atoms. The adsorption energies show that all these atoms can chemically adsorb on MX_2 monolayer even at room temperature. At the same time, the structure of MX_2 monolayer near the adatom has also been slightly distorted.

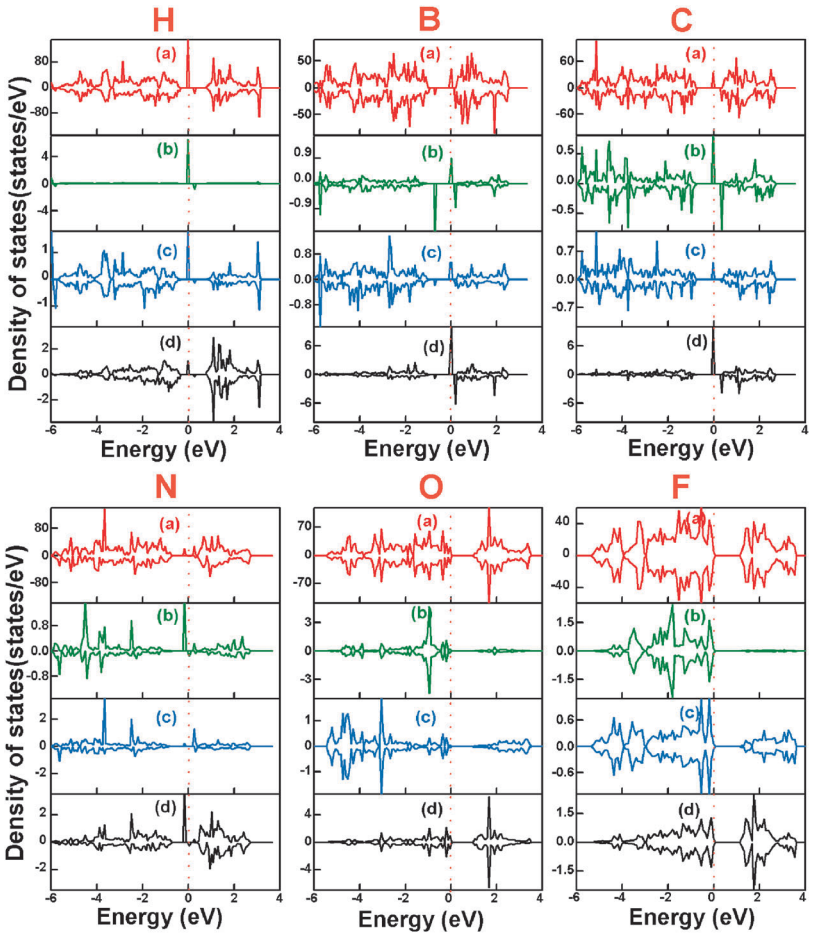

Fig. 7 The total DOS and the corresponding PDOS of H-, B-, C-, N-, O-, and F-adsorbed $MoTe_2$ monolayers. The upper most plane is the total DOS (a). The planes of (b), (c), and (d) are the p states of the adatom (s states for H), p states of the nearest Te atom, and d states of the nearest Mo atom, respectively. The vertical dashed line represents the Fermi level.

The spin unrestricted calculations show that the magnetic moments per 4×4 supercell are 1.0, 1.0, 2.0, 1.0, and 1.0 μ_B for H-, B-, C-, N-, and F-adsorbed WS_2 and $MoSe_2$ monolayers, respectively. While for O-adsorbed case, no spin-polarization can be obtained. To verify these systems are indeed magnetic, we also perform the spin restricted calculations on these cases. The ground state of H-, B-, C-, N-, and F-adsorbed WS_2 and $MoSe_2$ monolayers are magnetic because the spin-polarized state is more stable in energy than the spin-unpolarized one, while an equivalent total energy between spin-polarized and spin-unpolarized states was obtained for the O-adsorbed cases. It is noted that, similar to the H- and F-adsorbed graphene,[16,39] all the cases have integer number of unpaired spin in the supercell. As listed in Tables 2 and 3, the contributions of the adatoms H, B, C, N, and F to the total magnetic moments are 5, 2.7, 1.9, 48.5, and 29.5% for WS_2 monolayer case, respectively, while those of 5.4, 1, 2.3, 62.2, and 27.4% for the H-, B-, C-, N-, and F-adsorbed $MoSe_2$ monolayer. Moreover, the large spatial extensions of spin density have been observed in H- and F-absorbed WS_2 and $MoSe_2$ monolayers, which is important to achieve a long-range magnetic coupling interaction at low defect concentrations, while the B-, C-, and N-absorbed WS_2 and $MoSe_2$ monolayer sheets have rather small spatial extensions, especially for the case of N-absorption. As in the two systems discussed above, the spin-polarization shows that the total magnetic moments of H-, B-, C-, and N-adsorbed $MoTe_2$ monolayer are 1.0, 1.0, 2.0, and 1.0 μ_B, respectively, and the corresponding contribution of the adatoms H, B, C, and N to the total magnetic moments are 9, 1, 3, and 14%, respectively. It is interesting that, unlike F-adsorbed WS_2 and $MoSe_2$ monolayer sheets, F adsorption induces no magnetism in the $MoTe_2$ monolayer, which can be assigned as the different adsorption position. Meanwhile, the large spatial extension of spin density occurs in the H-absorbed $MoTe_2$ monolayer, and rather small spatial extension appears in B-, C-, and N-absorbed $MoTe_2$ monolayers. In order to further understand the changes of the electronic structure in nonmetal element adsorbed MX_2 monolayer, the density of states (DOS) of H-, B-, C-, N-, O-, and F-adsorbed WS_2, $MoSe_2$, and $MoTe_2$ nanosheets in their most stable configurations are shown in Fig. 5, 6 and 7, respectively. The magnetic couplings of H- or F-absorbed MoX_2 monolayers are examined by doubling the previous geometry in x direction and setting the initial magnetic moments to be FM and AFM respectively. Weak AFM coupling are observed at a distance of 12.74 Å for H-absorbed WS_2, $MoSe_2$, and $MoTe_2$ monolayers and F-adsorbed WS_2 and $MoSe_2$ monolayers. We can assign this kind of long-range weak AFM coupling at a

distance of 12.74 Å as the large spatial extensions of spin density just discussed above. These findings suggest a new route to facilitate the design of spintronic devices. Experimental tests for our results are called for.

IV. Summary

In summary, we investigated the electronic and magnetic properties of perfect, vacancy-doped, and nonmetal (H, B, C, N, O, and F) adsorbed $MoSe_2$, $MoTe_2$ and WS_2 nanosheets using first-principles calculations within the spin DFT. Our findings can be summarized into three main points.

(1) Perfect $MoSe_2$, $MoTe_2$ and WS_2 exhibit quantum confinement-induced indirect-direct-gap crossover characters. It is evident that the monolayer sheets are semiconductors with direct band gaps of 1.80, 1.44, and 1.07 eV for WS_2, $MoSe_2$, and $MoTe_2$ monolayers, respectively, whereas for the three-dimensional MX_2 the bands are indirect. This observation indicates that quantum confinement in layered d-electron materials, like $MoSe_2$, $MoTe_2$ and WS_2, provides new opportunities for design of the electronic structure of matter at the nanoscale.

(2) For the deficient $MoSe_2$, $MoTe_2$ and WS_2 monolayer sheets, surprisingly, only Mo vacancy in $MoSe_2$ can induce spin-polarization, and results in long-range antiferromagnetic coupling between the local moments even at a distance of above 13 Å due to the large spatial extensions of spin density. Other neutral native vacancies can not lead to magnetism in these systems.

(3) H, B, C, N, O and F chemically adsorption on $MoSe_2$, $MoTe_2$ and WS_2 nanosheets would induce total magnetic moment of 1.0, 1.0, 2.0 and 1.0 μ_B per 4×4 supercell, respectively. Surprisingly, H absorption on WS_2, $MoSe_2$, and $MoTe_2$ monolayers results in large spatial extensions of spin density and weak AFM coupling between local magnetic moments even at the distance of above 12.74 Å, and so does F adsorption on WS_2 and $MoSe_2$ monolayers.

The results may provide useful guidelines for understanding these newly synthesized two-dimensional nanosheets. And it is believed that the nature of the vacancy-doping and nonmetal element-adsorption giving rise to magnetism in these systems will soon be identified by experiments.

Acknowledgements

This work is supported by the National Natural Science Foundation of China under Grant 10774091 and 20973102, National Basic Research Program of China (973 Program, Grant 2007CB613302).

References

1 B. Radisavljevic, A. Radenovic, J. Brivio, V. Giacometti and A. Kis, *Nat. Nanotechnol.*, 2011, **6**, 147.
2 X. Zong, H. Yan, G. Wu, G. Ma, F. Wen, L. Wang and C. Li, *J. Am. Chem. Soc.*, 2008, **130**, 7176.
3 R. V. Kasowski, *Phys. Rev. Lett.*, 1973, **30**, 1175.
4 L. F. Mattheis, *Phys. Rev. Lett.*, 1973, **30**, 784.
5 Jonathan N. Coleman, *et al.*, *Science*, 2011, **331**, 568.
6 J. He, K. Wu, R. Sa, Q. Li and Y. Wei, *Appl. Phys. Lett.*, 2010, **96**, 082504.
7 K. F. Mak, C. Lee, J. Hone, J. Shan and T. F. Heinz, *Phys. Rev. Lett.*, 2010, **105**, 136805.
8 C. N. R. Rao and A. Nag, *Eur. J. Inorg. Chem.*, 2010, 4244.
9 A. Splendiani, L. Sun, Y. Zhang, T. Li, J. Kim, C. Chim, G. Galli and F. Wang, *Nano Lett.*, 2010, **10**, 1271.
10 C. Shahar, R. Levi, S. R. Cohen and R. Tenne, *J. Phys. Chem. Lett.*, 2010, **1**, 540.
11 H. S. S. Ramakrishna Matte, A. Gomathi, Arun K. Manna, Dattatray J. Late, Ranjan Datta, Swapan K. Pati and C. N. R. Rao, *Angew. Chem.*, 2010, **122**, 4153.
12 A. Castellanos-Gomez, N. Agraït and G. Rubio-Bollinger, *Appl. Phys. Lett.*, 2010, **96**, 213116.
13 K. Novoselov, D. Jiang, F. Schedin, T. Booth, V. Khotkevich, S. Morozov and A. Geim, *Proc. Natl. Acad. Sci. U. S. A.*, 2005, **102**, 10451.
14 Y. F. Li, Z. Zhou, S. B. Zhang and Z. F. Chen, *J. Am. Chem. Soc.*, 2008, **130**, 16739.
15 S. Lebègue and O. Eriksson, *Phys. Rev. B: Condens. Matter Mater. Phys.*, 2009, **79**, 115409.
16 Y. D. Ma, Y. Dai, M. Guo, C. N. Niu, L. Yu and B. B. Huang, *Nanoscale*, 2011, **3**, 2301.
17 Y. G. Zhou, X. T. Zu, F. Gao, H. F. Lv and H. Y. Xiao, *Appl. Phys. Lett.*, 2009, **95**, 123119.
18 O. V. Yazyev and L. Helm, *Phys. Rev. B: Condens. Matter Mater. Phys.*, 2007, **75**, 125408.
19 M. Wu, E.-Z. Liu and J. Z. Jiang, *Appl. Phys. Lett.*, 2008, **93**, 082504.
20 K. S. Yang, R. Wu, L. Shen, Y. P. Feng, Y. Dai and B. B. Huang, *Phys. Rev. B: Condens. Matter Mater. Phys.*, 2010, **81**, 125211.
21 J. J. Attema, G. A. deWijs, G. R. Blake and R. A. de Groot, *J. Am. Chem. Soc.*, 2005, **127**, 16325.
22 W. Kohn and L. J. Sham, *Phys. Rev.*, 1965, **140**, A1133.
23 G. Kresse and D. Joubert, *Phys. Rev. B: Condens. Matter Mater. Phys.*, 1999, **59**, 1758.
24 G. Kresse and J. Furthmüller, *Phys. Rev. B: Condens. Matter*, 1996, **54**, 11169.
25 G. Kresse and J. Furthmüller, *Comput. Mater. Sci.*, 1996, **6**, 15.
26 J. P. Perdew, K. Burke and M. Ernzerhof, *Phys. Rev. Lett.*, 1996, **77**, 3865.
27 H. J. Monkhorst and J. D. Pack, *Phys. Rev. B: Solid State*, 1976, **13**, 5188.
28 S. W. Fan, K. L. Yao and Z. L. Liu, *Appl. Phys. Lett.*, 2009, **94**, 152506.
29 Y. D. Ma, Y. Dai and B. B. Huang, *Comput. Mater. Sci.*, 2011, **50**, 1661.
30 A. H. Reshak and S. Auluck, *Phys. Rev. B: Condens. Matter Mater. Phys.*, 2005, **71**, 155114.
31 L. Kulyuk, D. Dumcehnko, E. Bucher, K. Friemelt, O. Schenker, L. Charron, E. Fortin and T. Dumouchel, *Phys. Rev. B: Condens. Matter Mater. Phys.*, 2005, **72**, 075336.
32 K. Albe and A. Klein, *Phys. Rev. B: Condens. Matter*, 2002, **66**, 073413.
33 T. S. Li and G. L. Galli, *J. Phys. Chem. C*, 2007, **111**, 16192.
34 S. Lebegue and O. Eriksson, *Phys. Rev. B: Condens. Matter Mater. Phys.*, 2009, **79**, 115409.
35 Droghetti, C. D. Pemmaraju and S. Sanvito, *Phys. Rev. B: Condens. Matter Mater. Phys.*, 2010, **81**, 092403.
36 J. L. Gavartin, D. Muñoz Ramo and A. L. Shluger, *Appl. Phys. Lett.*, 2006, **89**, 082908.
37 A. M. Stoneham, J. Gavartin, A. L. Shluger, A. V. Kimmel, D. Munõz Ramo, H. M. Rønnow, G. Aeppli and C. Renner, *J. Phys.: Condens. Matter*, 2007, **19**, 255208.
38 P. Dev, Y. Xue and P. Zhang, *Phys. Rev. Lett.*, 2008, **100**, 117204.
39 D. W. Boukhvalov, M. I. Katsnelson and A. I. Lichtenstein, *Phys. Rev. B: Condens. Matter Mater. Phys.*, 2008, **77**, 35427.